

Cite this: *Chem. Sci.*, 2024, 15, 9318

All publication charges for this article have been paid for by the Royal Society of Chemistry

# Systemic regulation of binding sites in porous coordination polymers for ethylene purification from ternary C2 hydrocarbons†

Yi Li,<sup>a</sup> Yanxin Wu,<sup>a</sup> Jiaxin Zhao,<sup>a</sup> Jingui Duan<sup>ID</sup>\*<sup>ab</sup> and Wanqin Jin<sup>ID</sup>\*<sup>a</sup>

The global demand for poly-grade ethylene (C<sub>2</sub>H<sub>4</sub>) is increasing annually. However, the energy-saving purification of this gas remains a major challenge due to the similarity in molecular properties among the ternary C2 hydrocarbons. To address this challenge, we report an approach of systematic tuning of the pore environment with organic sites (from –COOH to –CF<sub>3</sub>, then to –CH<sub>3</sub>) in porous coordination polymers (PCPs), of which NTU-73-CH<sub>3</sub> shows remarkable capability for the direct production of poly-grade C<sub>2</sub>H<sub>4</sub> from ternary C2 hydrocarbons under ambient conditions. In comparison, the precursor structure of NTU-73-COOH is unable to purify C<sub>2</sub>H<sub>4</sub>, while NTU-73-CF<sub>3</sub> shows minimal ability to harvest C<sub>2</sub>H<sub>4</sub>. This is because the changed binding sites in the NTU-73-series not only eliminate the channel obstruction caused by the formation of gas clusters, but also enhance the interaction with acetylene (C<sub>2</sub>H<sub>2</sub>) and ethane (C<sub>2</sub>H<sub>6</sub>), as validated by *in situ* crystallographic and Raman analysis. Our findings, in particular the systematic tuning of the pore environment and the efficient C<sub>2</sub>H<sub>4</sub> purification by NTU-73-CH<sub>3</sub>, provide a blueprint for the creation of advanced porous families that can handle desired tasks.

Received 22nd April 2024

Accepted 10th May 2024

DOI: 10.1039/d4sc02659d

rsc.li/chemical-science

## Introduction

Ethylene (C<sub>2</sub>H<sub>4</sub>) is used as an important building block in industry for the production of value-added organics.<sup>1–3</sup> Currently, C<sub>2</sub>H<sub>4</sub> is mainly obtained by separating the downstream of cracking of naphtha, C2 hydrocarbon gas mixtures during the steam cracking process.<sup>4–6</sup> Typically, acetylene (C<sub>2</sub>H<sub>2</sub>) is removed by solvent extraction or catalytic hydrogenation, which requires large equipment, as well as large amounts of solvents or higher temperature.<sup>7,8</sup> Subsequently, ethane (C<sub>2</sub>H<sub>6</sub>) is removed through cryogenic distillation, a type of huge energy-consuming process.<sup>9</sup>

The energy-intensive and cost-effective processes have spurred research into the development of energy-efficient approaches.<sup>10</sup> Adsorptive separation, with a significant character of energy efficiency, has been considered as a kind of alternative or transition technology.<sup>11</sup> Porous coordination polymers (PCPs),<sup>12–16</sup> covalent organic frameworks (COFs),<sup>17,18</sup> zeolites,<sup>19–21</sup> and carbon materials<sup>22</sup> have been explored for gas

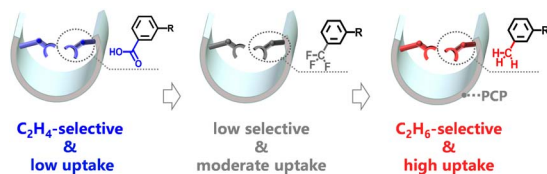
separation. Thanks to the rational pore tuning and straightforward pore functionalization, PCPs have shown good performance as adsorbents for various gas separations, but only a few examples can purify C<sub>2</sub>H<sub>4</sub> from binary mixtures containing C<sub>2</sub>H<sub>2</sub> or C<sub>2</sub>H<sub>6</sub>. However, from an energy point of view, it is crucial to remove both by-products in one-step with an adsorbent, but the challenge is enormous.<sup>23–25</sup>

In general, the preferential adsorption of C<sub>2</sub>H<sub>2</sub> over C<sub>2</sub>H<sub>4</sub> requires the pore to contain highly polar sites (such as inorganic anionic pillars and open metal sites) due to the larger quadrupole moment ( $7.2 \times 10^{-26}$  vs.  $1.5 \times 10^{-26}$  esu cm<sup>2</sup>) and higher acidity (pK<sub>a</sub>: 45 vs. 26) of C<sub>2</sub>H<sub>2</sub>, resulting in strong host–C<sub>2</sub>H<sub>2</sub> electrostatic interactions.<sup>26</sup> Conversely, the greater polarizability of C<sub>2</sub>H<sub>6</sub> ( $44.7 \times 10^{-25}$  vs.  $42.5 \times 10^{-25}$  cm<sup>3</sup>) contributes to the relatively weak van der Waals interactions with the structural framework modified low polarity sites.<sup>27–30</sup> To address this conflict, very few studies have been reported, primarily by exploiting the supramolecular interactions. The early framework of TJT-100 demonstrates the simultaneous capture of C<sub>2</sub>H<sub>2</sub> and C<sub>2</sub>H<sub>6</sub> through a hierarchy of interactions between the electronegative carboxylate O atoms and the gases.<sup>11</sup> A similar interaction has also been observed in NPU-1.<sup>31</sup> By incorporating the –NH<sub>2</sub> group or exposing the N site, UiO-67-NH<sub>2</sub> and Al-PyDC also show preferential adsorption of C<sub>2</sub>H<sub>2</sub> and C<sub>2</sub>H<sub>6</sub>.<sup>32,33</sup> Additionally, the cyclopentadiene-cobalt functional group in the UPC-series allows for efficient separation of C2 hydrocarbon mixtures. More promisingly, the synergistic sorbent separation technology (also called Lego-brick strategy) enables the production of high-purity C<sub>2</sub>H<sub>4</sub> from a quaternary mixture of

<sup>a</sup>State Key Laboratory of Materials-Oriented Chemical Engineering, Nanjing Tech University, Nanjing 211816, China. E-mail: duanjingui@njtech.edu.cn; wqjin@njtech.edu.cn

<sup>b</sup>State Key Laboratory of Chemistry and Utilization of Carbon Based Energy Resources, College of Chemistry, Xinjiang University, Urumqi, 830017, China

† Electronic supplementary information (ESI) available: Synthesis and characterization of the three crystals, PXRD, TGA, IR, sorption isotherms, IAST, breakthrough experiments and fitting parameters. CCDC 2337168–2337175. For ESI and crystallographic data in CIF or other electronic format see DOI: <https://doi.org/10.1039/d4sc02659d>



Scheme 1 Systemic tuning of the functional sites in PCPs for efficient  $C_2H_4$  purification.

$C_2H_6/C_2H_4/C_2H_2/CO_2$  by utilizing tandem packing of carefully selected PCPs, with each PCP acting as a separator for binary mixtures.<sup>25,34</sup> Although these individual materials exhibit the desired functions, further systematic exploration is urgently needed due to the abundance and facile tunability of the supramolecular sites.

We are interested in the separation of light hydrocarbons using finely designed PCPs.<sup>35–39</sup> Recently, we have reported a new family of PCPs with crab-like carboxylic pincers, which allows for high  $C_2H_2/C_2H_4$  selectivity and an unprecedented ability to obtain high-purity forms of both gases.<sup>40</sup> However, the strong binding interaction allows the absorbed  $C_2H_2$  to form a tetrameric gas cluster at the channel neck, which strongly blocks the accessibility of the adjacent large cavity. Inspired by the unique porous nature of NTU-73 and also by the function of supramolecular sites, we report here a systematic tuning of functional sites in this porous platform, where the carboxylic pincers on the pore wall (corresponding L1: 3,5-di(1*H*-imidazol-1-yl)benzoic acid) were replaced with  $-CF_3$  (corresponding L2: 1,1'-(5-(trifluoromethyl)-1,3-phenylene)bis(1*H*-imidazole)) or  $-CH_3$  (corresponding L3: 1,1'-(5-methyl-1,3-phenylene)bis(1*H*-imidazole)) (Scheme 1). The highly stable NTU-73- $CH_3$  exhibits a remarkable ability to directly produce poly-grade  $C_2H_4$  from ternary C2 hydrocarbons, while, NTU-73- $CF_3$  and NTU-73-COOH can only exhibit minimal capacity or are unable to achieve  $C_2H_4$  purification at all. These results reflect the positive effect of changing functional sites on strengthening the host-guest interactions and the stability of the framework.

## Experimental section

General procedures of the experiments and simulation are available in the ESI.†

### Synthesis of NTU-73-series

**Synthesis of NTU-73-COOH.** NTU-73-COOH was synthesized according to our previous work.<sup>40</sup>

**Synthesis of NTU-73- $CF_3$ .**  $Cu(BF_4)_2 \cdot 6H_2O$  (10 mg, 0.039 mmol), L2 (5 mg, 0.018 mmol) and  $H_2ZrF_6$  (50  $\mu$ L, 45%) were mixed in *N,N'*-dimethylacetamide (DMA)/ $H_2O$ /ethanol (EtOH) (0.5/0.25/0.75, v/v/v, 1.5 mL) and reacted at 90 °C for 2 days to obtain blue block crystals. After cooling down, the crystals were washed three times with fresh DMA (yield: ~52%, based on L2).

**Synthesis of NTU-73- $CH_3$ .**  $Cu(BF_4)_2 \cdot 6H_2O$  (10 mg, 0.039 mmol), L3 (5 mg, 0.022 mmol) and  $H_2ZrF_6$  (50  $\mu$ L, 45%) were added to the DMA/ $H_2O$ /EtOH (0.5/0.25/0.75, 1.5 mL) mixed

solvent and reacted at 90 °C for 2 days to give blue block crystals. After cooling down, the crystals were washed three times with fresh DMA (yield: ~60%, based on L3).

## Results and discussion

### Crystal structures and characterization

Solvent-thermal reactions of copper(II) hexafluorozirconium with corresponding ligands yielded polyhedron-shaped crystals (NTU-73-series). These crystals all crystallized in a tetragonal  $I4_122$  space group with the formula of  $[Cu(L)_2ZrF_6] \cdot xGuest$  (Table S1†). Two of our newly synthesized crystals (NTU-73- $CF_3$  and NTU-73- $CH_3$ ) have the same coordination mode as that of NTU-73-COOH. The asymmetric unit of all three PCPs consists of one ligand, half a  $Cu^{2+}$  ion and half a  $ZrF_6^{2-}$  anion. Each Cu node is coordinated by two F atoms from the two  $ZrF_6^{2-}$  anions and four imidazole N atoms from four ligands (Fig. S3–S5†). Additionally, two helical chains linked by  $ZrF_6^{2-}$  anions are present in the frameworks (Fig. S6†). Differently, the carboxylic-modified channel wall observed from two different directions in NTU-73-COOH has been replaced by a couple of  $-CF_3$  or  $-CH_3$  groups in NTU-73- $CF_3$  and NTU-73- $CH_3$  (Fig. S7–S12†), respectively. Furthermore, there is an overall trend of increasing pore size (NTU-73-COOH:  $4.5 \times 5.2 \text{ \AA}^2$  and  $3.9 \times 5.6 \text{ \AA}^2$ ; NTU-73- $CF_3$ :  $3.7 \times 5.2 \text{ \AA}^2$  and  $4.2 \times 7.8 \text{ \AA}^2$ ; NTU-73- $CH_3$ :  $4.4 \times 5.4 \text{ \AA}^2$  and  $6.2 \times 9.2 \text{ \AA}^2$ ) as the functional group size gradually decreases (Fig. 1). Considering the unique ability of NTU-73-COOH to separate  $C_2H_2/C_2H_4$  and the systematic changes in the pore environment, including binding sites and pore size, we expected this platform to be highly efficient for the C2 ternary mixture separation. The phase purity of the crystals was confirmed by powder X-ray diffraction (PXRD) as the diffraction peaks of the synthesized and activated NTU-73-series were in good agreement with the simulated patterns (Fig. S13–S15†).

### Pore evaluation

The permanent porosity of the NTU-73-series was investigated through  $N_2$  (77 K) and  $CO_2$  (195 K) adsorption measurements (Fig. 2a and S22†). Although NTU-73-COOH exhibits negligible  $N_2$  uptake, the two newly prepared PCPs show improved  $N_2$  adsorption, with maximum uptakes of 193 and 295  $cm^3 g^{-1}$ , respectively. Interestingly, all three PCPs show type-I and significant  $CO_2$  adsorption isotherms. The maximum uptake increases from 63 (NTU-73-COOH) to 250  $cm^3 g^{-1}$  (NTU-73- $CH_3$ ). For consistency, the Brunauer–Emmett–Teller surface areas of the NTU-73-series were calculated based on  $CO_2$  isotherms. The BET surface areas of the NTU-73-series were calculated to be 228, 889 and 1078  $m^2 g^{-1}$ , respectively, with corresponding pore volumes of 0.039, 0.153 and 0.185  $m^3 g^{-1}$  (Table S2†). Additionally, the pore size distribution is consistent with the crystal structures, verifying the impact of the functional groups on pore size tuning (Fig. S23†).

### Single-component adsorption and selectivity

Single-component adsorption isotherms of  $C_2H_2$ ,  $C_2H_4$  and  $C_2H_6$  were collected for the three PCPs (Fig. 2b–d and S24–



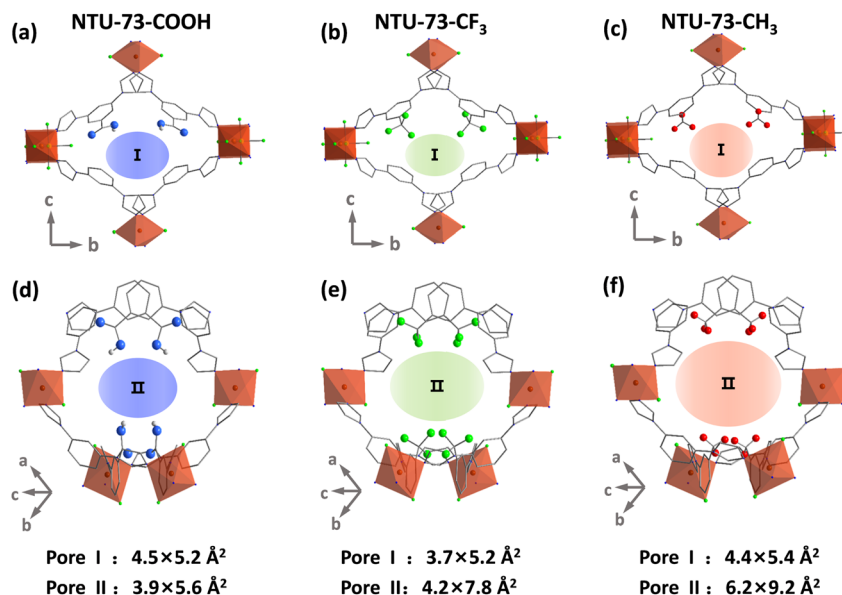


Fig. 1 Structure of the NTU-73-series: local views of the nanospace of NTU-73-COOH (a and d), NTU-73-CF<sub>3</sub> (b and e) and NTU-73-CH<sub>3</sub> (c and f) in different directions.

S35†), respectively. With the carboxylate pincers, exposed in the nanochannel, **NTU-73-COOH** shows the lowest gas uptake (C<sub>2</sub>H<sub>2</sub>: 32.3 cm<sup>3</sup> g<sup>−1</sup>, C<sub>2</sub>H<sub>4</sub>: 12.9 cm<sup>3</sup> g<sup>−1</sup> and C<sub>2</sub>H<sub>6</sub>: 11.8 cm<sup>3</sup> g<sup>−1</sup>) among the three PCPs. Not only that, the adsorption capacity of C<sub>2</sub>H<sub>4</sub> is slightly higher than that of C<sub>2</sub>H<sub>6</sub>, indicating an impossible harvesting of pure C<sub>2</sub>H<sub>4</sub> in one-step from the ternary C<sub>2</sub> mixtures, although it shows promising ability in binary C<sub>2</sub>H<sub>2</sub>/C<sub>2</sub>H<sub>4</sub> separation. After replacing the −COOH groups with −CF<sub>3</sub> groups, **NTU-73-CF<sub>3</sub>** shows a significantly increased gas uptake at 100 kPa (C<sub>2</sub>H<sub>2</sub>: 77.7 cm<sup>3</sup> g<sup>−1</sup>, C<sub>2</sub>H<sub>4</sub>: 62.0 cm<sup>3</sup> g<sup>−1</sup>, and C<sub>2</sub>H<sub>6</sub>: 62.7 cm<sup>3</sup> g<sup>−1</sup>), in which the C<sub>2</sub>H<sub>6</sub> uptake is slightly higher

than that of C<sub>2</sub>H<sub>4</sub>. Comparing the structural nature of the above two, the decrease in the polarity of the pore surface could alter the sequence of host–C<sub>2</sub>H<sub>4</sub> and –C<sub>2</sub>H<sub>6</sub> interactions. As expected, the adsorption capacities of C<sub>2</sub> gases show a further increase in **NTU-73-CH<sub>3</sub>** (C<sub>2</sub>H<sub>2</sub>: 98.0 cm<sup>3</sup> g<sup>−1</sup>; C<sub>2</sub>H<sub>4</sub>: 77.8 cm<sup>3</sup> g<sup>−1</sup>; C<sub>2</sub>H<sub>6</sub>: 89.9 cm<sup>3</sup> g<sup>−1</sup>), particularly, the C<sub>2</sub>H<sub>6</sub> uptake is higher than that of C<sub>2</sub>H<sub>4</sub> (12.1 cm<sup>3</sup> g<sup>−1</sup>, 100 kPa, 298 K). Notably, this uptake difference is much higher than that of the benchmark materials of MOF-303 (−0.5 cm<sup>3</sup> g<sup>−1</sup>),<sup>41</sup> NPU-1 (6.7 cm<sup>3</sup> g<sup>−1</sup>),<sup>31</sup> TJT-100 (5.8 cm<sup>3</sup> g<sup>−1</sup>),<sup>11</sup> and is approaching that of Al-PyDC (17.0 cm<sup>3</sup> g<sup>−1</sup>, 296 K)<sup>33</sup> and UPC-612 (17.5 cm<sup>3</sup> g<sup>−1</sup>)<sup>6</sup> (Table S3†). In addition,

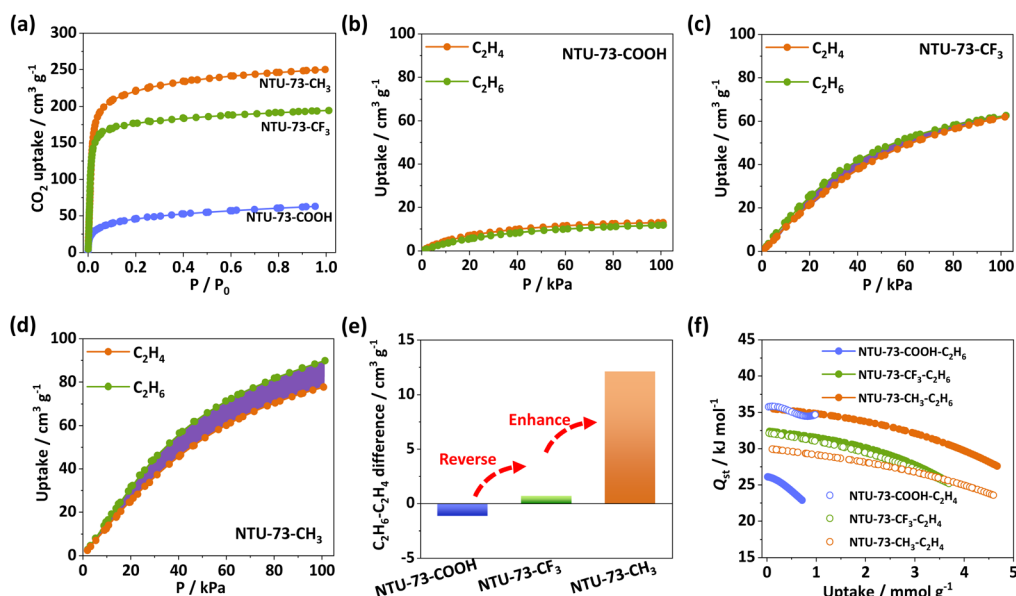


Fig. 2 CO<sub>2</sub>-adsorption isotherms of the NTU-73-series at 195 K (a). C<sub>2</sub>H<sub>4</sub> and C<sub>2</sub>H<sub>6</sub> adsorption isotherms of NTU-73-COOH (b), NTU-73-CF<sub>3</sub> (c), and NTU-73-CH<sub>3</sub> (d) at 298 K. Uptake difference (e) and isosteric heats (f) of the three PCPs.

despite the gradual decrease in pore channel polarity,  $C_2H_2$  uptake is always higher than that of  $C_2H_4$ , about  $20.0\text{ cm}^3\text{ g}^{-1}$ , in the **NTU-73-series** (Fig. 2e and S36†). In other words, systematically tuned organic sites endow significant functional changes, where **NTU-73-CH<sub>3</sub>** is expected to achieve efficient  $C_2H_4$  purification from C2 ternary mixtures.

### Static adsorption selectivity and isosteric heats

To further evaluate the gas separation performance, the adsorption selectivities of  $C_2H_6/C_2H_4$  and  $C_2H_2/C_2H_4$  at 298 K were calculated *via* the ideal adsorbed solution theory (IAST) after fitting the single-component adsorption isotherms to the Langmuir–Freundlich equation (Fig. S37–S49†). For the equimolar  $C_2H_6/C_2H_4$  mixtures, the adsorption selectivity values were found to be 0.66 for **NTU-73-COOH**, 1.18 for **NTU-73-CF<sub>3</sub>** and 1.33 for **NTU-73-CH<sub>3</sub>**. Importantly, the selectivity of **NTU-73-CH<sub>3</sub>** is higher than that of TJT-100 (1.2) and NPU-1 (1.32), and close to that of UPC-612 (1.4), MOF-303 (1.7), Al-PyDC (1.9, 296 K) under almost the same conditions (Table S3†). Additionally, among the top-tier ( $C_2H_6$ – $C_2H_4$  uptake difference larger than  $10\text{ cm}^3\text{ g}^{-1}$ )  $C_2H_2$ – $C_2H_6$ -selective adsorbents, the  $C_2H_2/C_2H_4$  (1/99, v/v) selectivity (3.2 at 298 K, 100 kPa) of **NTU-73-CH<sub>3</sub>** is only lower than that of Al-PyDC (4.3 at 296 K, 100 kPa) (Table S4†). Therefore, the high  $C_2H_6$ – $C_2H_4$  uptake difference and the good selectivities make **NTU-73-CH<sub>3</sub>** a promising candidate for  $C_2H_4$  purification from C2 ternary mixtures.

To evaluate the interaction strength of  $C_2H_2$ ,  $C_2H_4$  and  $C_2H_6$  in the **NTU-73-series**, the isosteric heat ( $Q_{st}$ ) was calculated after fitting the adsorption isotherms by the virial equation at 273, 283 and 298 K, respectively (Fig. 2f and S50–S59†). The  $Q_{st}$  value of  $C_2H_2$  (**NTU-73-COOH**:  $41.00\text{ kJ mol}^{-1}$ , **NTU-73-CF<sub>3</sub>**:  $39.83\text{ kJ mol}^{-1}$ , **NTU-73-CH<sub>3</sub>**:  $37.06\text{ kJ mol}^{-1}$ ) is higher than that of  $C_2H_4$  (**NTU-73-COOH**:  $35.78\text{ kJ mol}^{-1}$ , **NTU-73-CF<sub>3</sub>**:  $32.12\text{ kJ mol}^{-1}$ , **NTU-73-CH<sub>3</sub>**:  $29.90\text{ kJ mol}^{-1}$ ) and  $C_2H_6$  (**NTU-73-COOH**:  $26.10\text{ kJ mol}^{-1}$ , **NTU-73-CF<sub>3</sub>**:  $32.39\text{ kJ mol}^{-1}$ , **NTU-73-CH<sub>3</sub>**:  $35.43\text{ kJ mol}^{-1}$ ) in the **NTU-73-series** at low coverage, while

an inversion of the host– $C_2H_4$  and host– $C_2H_6$  interactions was observed: a higher  $Q_{st}$  of  $C_2H_4$  over  $C_2H_6$  in **NTU-73-COOH** changes to a higher  $Q_{st}$  of  $C_2H_6$  over  $C_2H_4$  in **NTU-73-CH<sub>3</sub>**. These observations are consistent with the adsorption isotherms. In addition, these relatively low adsorption enthalpy values indicate a relatively low energy consumption for regeneration of the PCPs.

### Gas-loaded crystallographic and Raman analysis

The isosteric heat is a kind of statistical result, making it difficult to accurately describe the role of functional sites. Therefore, to better explore the reversal phenomenon of  $C_2H_4$  and  $C_2H_6$  adsorption and  $Q_{st}$  values, gas-loaded crystallographic analysis was performed at 298 K (Fig. 3 and Table S5†).<sup>42</sup> Despite the disordered nature, the trapped gases can be clearly found in these three PCPs. For **NTU-73-COOH**  $\supset C_2H_4$ , two  $C_2H_4$  molecules form three hydrogen bonds with the  $O_{COOH}$  of the free carboxylic piners, of which, the shortest distance is  $1.8973\text{ Å}$ . Meanwhile, intermolecular interactions ( $d_{C_2H_4-H\cdots C_2H_4}$ :  $2.3748$  to  $2.8025\text{ Å}$ ) have been found between these two molecules (Fig. 3a). For **NTU-73-COOH**  $\supset C_2H_6$ , two groups of hydrogen bonds ( $d_{C_2H_6-H\cdots O_{COOH}}$ :  $2.3338$  to  $2.9779\text{ Å}$  and  $d_{C_2H_6-H\cdots N_{imidazole}}$ ) with relatively longer distances were observed. In addition, the slightly larger distance leads to the disappearance of the intermolecular interactions (Fig. 3b). This clear change can therefore explain the fact that **NTU-73-COOH** binds  $C_2H_4$  more strongly than  $C_2H_6$ . However, in contrast to our expectation, the distance between the gases and the  $-CF_3$  group is relatively far. So as that, both molecules are located around the coordinated  $ZrF_6^{2-}$  ions. This is due to the relatively weak degree of electronegativity of  $F_{CF_3}$  compared to that of  $F_{ZrF_6}$ . However, the presence of the  $-CF_3$  group influences the configuration of the adsorbed gas molecules. As can be seen, the two F atoms of  $ZrF_6^{2-}$  form two hydrogen bonds with  $C_2H_4$  and  $C_2H_6$ , respectively. The shortest distances of the hydrogen bonds ( $d_{C_2H_6-H\cdots F_{ZrF_6}}$ :  $2.6094\text{ Å}$  and  $d_{C_2H_4-H\cdots F_{ZrF_6}}$ :  $2.6647$

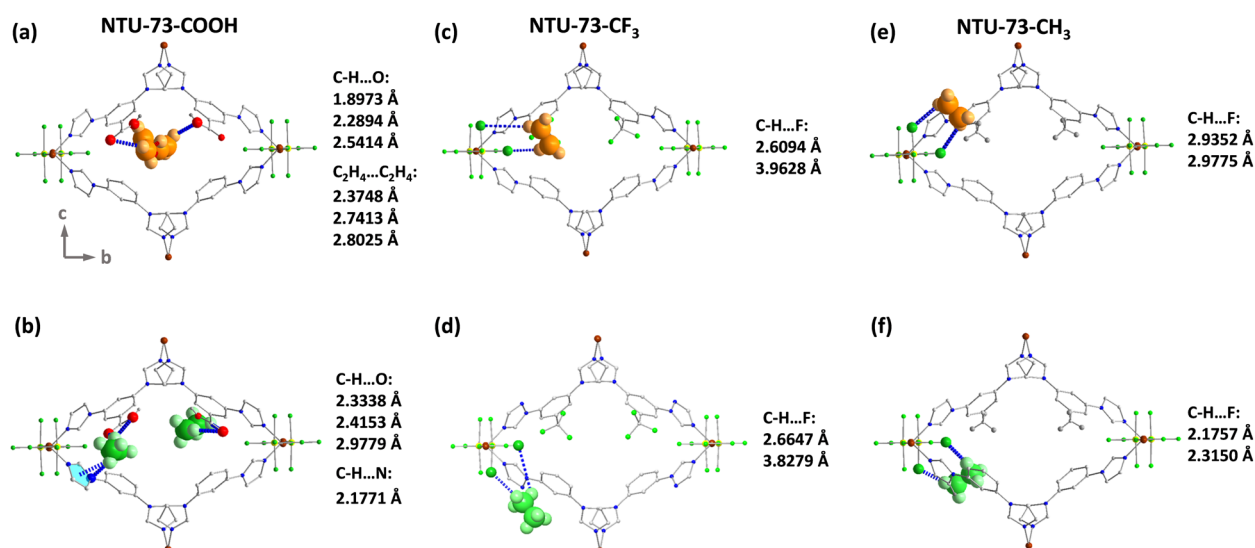


Fig. 3  $C_2H_4$ - and  $C_2H_6$ -loaded crystallographic analysis of **NTU-73-COOH** (a and b), **NTU-73-CF<sub>3</sub>** (c and d) and **NTU-73-CH<sub>3</sub>** (e and f).





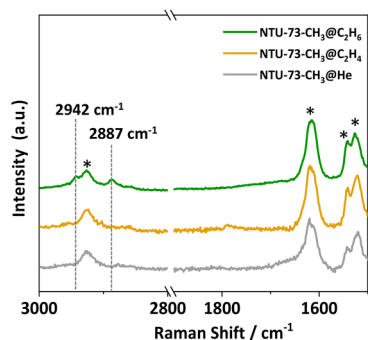


Fig. 4 Raman spectra of gas-loaded NTU-73-CH<sub>3</sub> (the peaks marked with \* derived from the framework).

Å) are very close to each other, indicating similar host-guest interactions (Fig. 3c and d). In NTU-73-CH<sub>3</sub>, both gases are also observed around the coordinated ZrF<sub>6</sub><sup>2-</sup> ions. Without the withdrawal effect of the organic F sites from -CF<sub>3</sub>, the configuration of the adsorbed C<sub>2</sub>H<sub>4</sub> shows a slight change, wherein the distance of the two hydrogen bonds (C<sub>2</sub>H<sub>4</sub>-H...F<sub>ZrF<sub>6</sub></sub>) becomes close to each other (2.9352 Å and 2.9775 Å) (Fig. 3e). Additionally, the end-on mode of C<sub>2</sub>H<sub>6</sub>-H...F<sub>ZrF<sub>6</sub></sub> in NTU-73-CF<sub>3</sub> changes to a chelate connection in NTU-73-CH<sub>3</sub>; particularly, the distance of the two C<sub>2</sub>H<sub>6</sub>-H...F<sub>ZrF<sub>6</sub></sub> (2.1757 Å and 2.3150 Å) is shorter than that of C<sub>2</sub>H<sub>6</sub>-H...F<sub>ZrF<sub>6</sub></sub> in NTU-73-CF<sub>3</sub> (Fig. 3f). Therefore, these results not only explain the phenomenon of the adsorption trend of C<sub>2</sub>H<sub>4</sub> and C<sub>2</sub>H<sub>6</sub> in NTU-73-series, but also can strengthen the molecular insights of fine-tuning the pore environment by functional organic groups.

Given the promising nature of NTU-73-CH<sub>3</sub>, the stabilizing effect of the pore environment towards C<sub>2</sub>H<sub>4</sub> and C<sub>2</sub>H<sub>6</sub> was

further evaluated by Raman spectra. After dosing a highly pure gas (He, C<sub>2</sub>H<sub>4</sub> or C<sub>2</sub>H<sub>6</sub>, 1 bar, 298 K) into the glass tube with fully activated NTU-73-CH<sub>3</sub>, respectively, the corresponding spectra were recorded in the range of 1000 to 4000 cm<sup>-1</sup> (Fig. 4 and S60†). As can be seen, the peaks at 2887 cm<sup>-1</sup> and 2942 cm<sup>-1</sup> belonging to the stretching vibration of C<sub>2</sub>H<sub>6</sub> have been identified,<sup>43</sup> but no additional peaks other than those belonging to NTU-73-CH<sub>3</sub> were observed under the C<sub>2</sub>H<sub>4</sub> atmosphere (theoretical position: 1689 cm<sup>-1</sup>). Therefore, it is clear that NTU-73-CH<sub>3</sub> not only has a relatively stronger host-C<sub>2</sub>H<sub>6</sub> interaction, but also can stabilize a certain number of C<sub>2</sub>H<sub>6</sub> molecules in a periodic arrangement, which is consistent with the results of the crystallographic analysis.

### Breakthrough experiments

To validate the separation performance under dynamic conditions, breakthrough experiments were conducted on the NTU-73-series (Fig. 5 and S61–S69†). All initially activated samples were loaded into the column and further activation was achieved by He sweeping until no signals were detected. Breakthrough experiments were then carried out using a binary mixture of C<sub>2</sub>H<sub>2</sub>/C<sub>2</sub>H<sub>4</sub> (1 : 99, v/v) at first, a typical industrial composition. Compared to NTU-73-COOH, both NTU-73-CF<sub>3</sub> and NTU-73-CH<sub>3</sub> showed a certain loss of breakthrough time interval, but still demonstrated the separation ability towards C<sub>2</sub>H<sub>2</sub>/C<sub>2</sub>H<sub>4</sub>. Further experiments were conducted on C<sub>2</sub>H<sub>6</sub>/C<sub>2</sub>H<sub>4</sub> mixtures. At a volume ratio of 1 : 15, C<sub>2</sub>H<sub>6</sub> breaks through slightly earlier than C<sub>2</sub>H<sub>4</sub> for the NTU-73-COOH sample bed. Interestingly, high purity C<sub>2</sub>H<sub>4</sub> can be obtained directly at the outlet of the NTU-73-CF<sub>3</sub> and NTU-73-CH<sub>3</sub> columns, of which, NTU-73-CH<sub>3</sub> has a longer C<sub>2</sub>H<sub>6</sub>-C<sub>2</sub>H<sub>4</sub> breakthrough interval than NTU-73-CF<sub>3</sub> (4.8 min g<sup>-1</sup> vs. 4.0 min g<sup>-1</sup>). To further

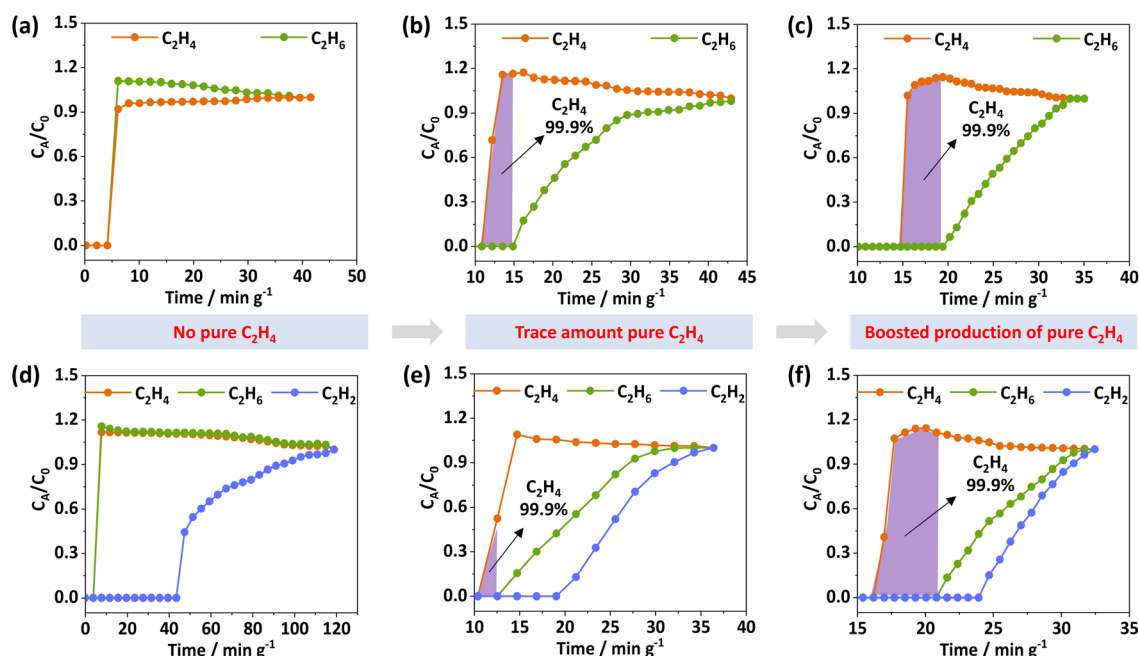


Fig. 5 Experimental breakthrough curves of NTU-73-COOH (a and d), NTU-73-CF<sub>3</sub> (b and e), and NTU-73-CH<sub>3</sub> (c and f) for C<sub>2</sub>H<sub>6</sub>/C<sub>2</sub>H<sub>4</sub> (1/9, v/v, 2 mL min<sup>-1</sup>) and C<sub>2</sub>H<sub>2</sub>/C<sub>2</sub>H<sub>6</sub>/C<sub>2</sub>H<sub>4</sub> (1/9/90, v/v/v, 2 mL min<sup>-1</sup>) mixtures, respectively at 298 K. The gas pressure is 1.4 bar for all experiments.



investigate the influence of ratio on this separation, a feed gas with a ratio of 1:9, the most common ratio found in the cracking process, was introduced into the column. **NTU-73-COOH** was unable to separate this mixture, while **NTU-73-CF<sub>3</sub>** and **NTU-73-CH<sub>3</sub>** retained their separation abilities. Among them, **NTU-73-CH<sub>3</sub>** showed the longest breakthrough time interval (4.6 min g<sup>-1</sup> vs. 2.7 min g<sup>-1</sup> vs. 0 min g<sup>-1</sup>), owing to its higher selectivity for C<sub>2</sub>H<sub>6</sub>/C<sub>2</sub>H<sub>4</sub> and its greater uptake capacity for C<sub>2</sub>H<sub>6</sub> (Fig. 5a–c). This trend was also observed in experiments using equimolar C<sub>2</sub>H<sub>6</sub>/C<sub>2</sub>H<sub>4</sub> mixtures.

Encouraged by the successful separation of the binary mixtures, C<sub>2</sub>H<sub>2</sub>/C<sub>2</sub>H<sub>4</sub> and C<sub>2</sub>H<sub>6</sub>/C<sub>2</sub>H<sub>4</sub>, the separation ability of the NTU-73-series towards ternary mixtures C<sub>2</sub>H<sub>2</sub>/C<sub>2</sub>H<sub>6</sub>/C<sub>2</sub>H<sub>4</sub> (1/9/90, v/v/v) was further investigated, respectively. As expected, both C<sub>2</sub>H<sub>6</sub> and C<sub>2</sub>H<sub>4</sub> elute out simultaneously from the **NTU-73-COOH** bed (Fig. 5d). Despite the separation potential, high-yield C<sub>2</sub>H<sub>4</sub> cannot be produced by **NTU-73-CF<sub>3</sub>** (Fig. 5e). Only **NTU-73-CH<sub>3</sub>** allows significant production of high purity (>99.9%) C<sub>2</sub>H<sub>4</sub> (0.52 mmol g<sup>-1</sup> (STP)) (Fig. 5f and S70†). This value is higher than that of CAU-23 (0.18 mmol g<sup>-1</sup>), TJT-100 (0.41 mmol g<sup>-1</sup>), and UPC-612 (0.47 mmol g<sup>-1</sup>), but lower than that of MOF-303 (1.35 mmol g<sup>-1</sup>) and Azole-Th-1 (1.34 mmol g<sup>-1</sup>) (Tables S3 and S4†).

### Stability and recyclability

Stability is another crucial factor in measuring the performance of adsorbents.<sup>44</sup> The crystals of **NTU-73-COOH**, **NTU-73-CF<sub>3</sub>** and **NTU-73-CH<sub>3</sub>** were immersed in chemical solutions (pH = 2, pH = 7 and pH = 12) for 3 days or exposed to air for 7 days, respectively. The PXRD patterns of the samples were then collected and compared with the simulated patterns (Fig. S71–S73†). The results reveal that some of the characteristic peaks of **NTU-73-COOH** and **NTU-73-CF<sub>3</sub>** were weakened or disappeared after immersion in certain solutions, in particular, the diffraction peaks almost completely disappeared in the alkaline solution (pH = 12), suggesting the structural instability. However, the crystals of **NTU-73-CH<sub>3</sub>** retained almost the same diffraction peaks after treatment under these harsh conditions. Additionally, the C<sub>2</sub>H<sub>6</sub> uptakes of these treated samples are nearly the same (Fig. S74†), indicating that the introduction of the hydrophobic –CH<sub>3</sub> group plays a crucial role in protecting the coordination bonds and then stabilizing the framework. Thanks to this good stability, **NTU-73-CH<sub>3</sub>** demonstrates no loss of performance during the cycling breakthrough experiments (Fig. S75†).

## Conclusions

In response to the demand for C<sub>2</sub>H<sub>4</sub> purification, we herein report an approach of systematic tuning of the porous environment with organic sites (from –COOH to –CF<sub>3</sub> and then to –CH<sub>3</sub>) in PCPs, wherein the highly stable **NTU-73-CH<sub>3</sub>** exhibits remarkable capability for direct production of poly-grade C<sub>2</sub>H<sub>4</sub> from ternary C2 hydrocarbons under ambient conditions. In addition, the molecular insights derived from *in situ* crystallographic and Raman analysis confirm the positive effect of the –CH<sub>3</sub> group in tuning the configuration and strength of the

adsorbed C<sub>2</sub>H<sub>4</sub> and C<sub>2</sub>H<sub>6</sub>. This study not only highlights the importance of systemic regulation, but also illustrates how changes in functional groups within PCPs can profoundly affect the host–guest interaction and separation performance. Moreover, the strategy of systematic organic functionalization can be extended to other porous families, offering a powerful tool for tailoring high-performance PCPs for desired applications.

## Data availability

All data can be found in the main text and ESI.†

## Author contributions

J. D. and W. J. conceived the idea of this work. Y. L. carried out the experiments and analyzed the results. J. D. and Y. L. wrote the paper. All authors gave valuable suggestions for the final draft.

## Conflicts of interest

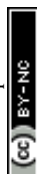
The authors declare no competing interests.

## Acknowledgements

We are thankful for the financial support of the National Natural Science Foundation of China (22171135), the National Natural Science Foundation of Jiangsu Province (BK20231269) and the State Key Laboratory of Materials-Oriented Chemical Engineering (SKL-MCE-23A18).

## References

- 1 S. Gong, C. Shao and L. Zhu, *Energy*, 2021, **217**, 119401.
- 2 S. M. Sadrameli, *Fuel*, 2016, **173**, 285–297.
- 3 G. D. Wang, Y. Z. Li, W. J. Shi, L. Hou, Y. Y. Wang and Z. Zhu, *Angew. Chem., Int. Ed.*, 2022, **61**, e202205427.
- 4 Z. B. Bao, D. Y. Xie, G. G. Chang, H. Wu, L. Y. Li, W. Zhou, H. L. Wang, Z. G. Zhang, H. B. Xing, Q. W. Yang, M. J. Zaworotko, Q. L. Ren and B. L. Chen, *J. Am. Chem. Soc.*, 2018, **140**, 4596–4603.
- 5 Q. Ding, Z. Zhang, Y. Liu, K. Chai, R. Krishna and S. Zhang, *Angew. Chem., Int. Ed.*, 2022, **61**, e202208134.
- 6 Y. T. Wang, C. L. Hao, W. D. Fan, M. Y. Fu, X. K. Wang, Z. K. Wang, L. Zhu, Y. Li, X. Q. Lu, F. N. Dai, Z. X. Kang, R. M. Wang, W. Y. Guo, S. Q. Hu and D. F. Sun, *Angew. Chem., Int. Ed.*, 2021, **60**, 11350–11358.
- 7 F. Studt, F. Abild-Pedersen, T. Bligaard, R. Z. Sorensen, C. H. Christensen and J. K. Nørskov, *Science*, 2008, **320**, 1320–1322.
- 8 Z. Xu, X. Xiong, J. Xiong, R. Krishna, L. Li, Y. Fan, F. Luo and B. Chen, *Nat. Commun.*, 2020, **11**, 3163–3172.
- 9 K. Z. Su, W. J. Wang, S. F. Du, C. Q. Ji and D. Q. Yuan, *Nat. Commun.*, 2021, **12**, 3703–3710.
- 10 J.-W. Cao, S. Mukherjee, T. Pham, Y. Wang, T. Wang, T. Zhang, X. Jiang, H.-J. Tang, K. A. Forrest, B. Space,



- M. J. Zaworotko and K.-J. Chen, *Nat. Commun.*, 2021, **12**, 6507–6515.
- 11 H. G. Hao, Y. F. Zhao, D. M. Chen, J. M. Yu, K. Tan, S. Q. Ma, Y. Chabal, Z. M. Zhang, J. M. Dou, Z. H. Xiao, G. Day, H. C. Zhou and T. B. Lu, *Angew. Chem., Int. Ed.*, 2018, **57**, 16067–16071.
- 12 Z. Q. Zhang, S. B. Peh, Y. X. Wang, C. J. Kang, W. D. Fan and D. Zhao, *Angew. Chem., Int. Ed.*, 2020, **59**, 18927–18932.
- 13 S. H. Yang, A. J. Ramirez-Cuesta, R. Newby, V. Garcia-Sakai, P. Manuel, S. K. Callear, S. I. Campbell, C. C. Tang and M. Schroder, *Nat. Chem.*, 2015, **7**, 121–129.
- 14 P. Q. Liao, W. X. Zhang, J. P. Zhang and X. M. Chen, *Nat. Commun.*, 2015, **6**, 8697–8706.
- 15 C. Gu, N. Hosono, J. J. Zheng, Y. Sato, S. Kusaka, S. Sakaki and S. Kitagawa, *Science*, 2019, **363**, 387–391.
- 16 Q. Ding, Z. Q. Zhang, C. Yu, P. X. Zhang, J. Wang, X. L. Cui, C. H. He, S. G. Deng and H. B. Xing, *Sci. Adv.*, 2020, **6**, 122617.
- 17 C. H. He, Y. Wang, Y. Chen, X. Q. Wang, J. F. Yang, L. B. Li and J. P. Li, *ACS Appl. Mater. Interfaces*, 2020, **12**, 52819–52825.
- 18 L. C. Jiang, Y. Y. Tian, T. Sun, Y. L. Zhu, H. Ren, X. Q. Zou, Y. H. Ma, K. R. Meihaus, J. R. Long and G. S. Zhu, *J. Am. Chem. Soc.*, 2018, **140**, 15724–15730.
- 19 Y. Z. Liu, Y. Wu, W. W. Liang, J. J. Peng, Z. Li, H. H. Wang, M. J. Janik and J. Xiao, *Chem. Eng. Sci.*, 2020, **220**, 115636.
- 20 P. J. Bereciartua, A. Cantin, A. Corma, J. L. Jorda, M. Palomino, F. Rey, S. Valencia, E. W. Corcoran, P. Kortunov, P. I. Ravikovitch, A. Burton, C. Yoon, Y. Wang, C. Paur, J. Guzman, A. R. Bishop and G. L. Casty, *Science*, 2017, **358**, 1068–1071.
- 21 Y. C. Chai, X. Han, W. Y. Li, S. S. Liu, S. K. Yao, C. Wang, W. Shi, I. Da-Silva, P. Manuel, Y. Q. Cheng, L. D. Daemen, A. J. Ramirez-Cuesta, C. C. Tang, L. Jiang, S. H. Yang, N. J. Guan and L. D. Li, *Science*, 2020, **368**, 1002–1006.
- 22 W. W. Liang, Y. Wu, H. Y. Xiao, J. Xiao, Y. W. Li and Z. Li, *Chem.-Eur. J.*, 2018, **64**, 3390–3399.
- 23 C. Xiao, J. D. Tian, Q. H. Chen and M. C. Hong, *Chem. Sci.*, 2024, **15**, 1570–1610.
- 24 P. Zhang, Y. Zhong, Y. Zhang, Z. Zhu, Y. Liu, Y. Su, J. Chen, S. Chen, Z. Zeng, H. Xing, S. Deng and J. Wang, *Sci. Adv.*, 2022, **8**, eabn9231.
- 25 K. J. Chen, D. G. Madden, S. Mukherjee, T. Pham, K. A. Forrest, A. Kumar, B. Space, J. Kong, Q. Y. Zhang and M. J. Zaworotko, *Science*, 2019, **366**, 241–246.
- 26 Q. Ding, Z. Q. Zhang, Y. L. Liu, K. G. Chai, R. Krishna and S. Zhang, *Angew. Chem., Int. Ed.*, 2022, **61**, e202208134.
- 27 M. Kang, S. Yoon, S. Ga, D. W. Kang, S. Han, J. H. Choe, H. Kim, D. W. Kim, Y. G. Chung and C. S. Hong, *Adv. Sci.*, 2021, **8**, 2004940.
- 28 M. J. Kang, D. W. Kang, J. H. Choe, H. Kim, D. W. Kim, H. Park and C. S. Hong, *Chem. Mater.*, 2021, **33**, 6193–6199.
- 29 J. Y. Pei, J. X. Wang, K. Shao, Y. Yang, Y. J. Cui, H. Wu, W. Zhou, B. Li and G. D. Qian, *J. Mater. Chem. A*, 2020, **8**, 3613–3620.
- 30 R. B. Lin, H. Wu, L. B. Li, X. L. Tang, Z. Q. Li, J. K. Gao, H. Cui, W. Zhou and B. L. Chen, *J. Am. Chem. Soc.*, 2018, **140**, 12940–12946.
- 31 B. Y. Zhu, J. W. Cao, S. Mukherjee, T. Pham, T. Zhang, T. Wang, X. Jiang, K. A. Forrest, M. J. Zaworotko and K. J. Chen, *J. Am. Chem. Soc.*, 2021, **143**, 1485–1492.
- 32 X. W. Gu, J. X. Wang, E. Y. Wu, H. Wu, W. Zhou, G. D. Qian, B. L. Chen and B. Li, *J. Am. Chem. Soc.*, 2022, **144**, 2614–2623.
- 33 E. Wu, X.-W. Gu, D. Liu, X. Zhang, H. Wu, W. Zhou and G. Qian, *Nat. Commun.*, 2023, **14**, 6146–6157.
- 34 H. R. Sun, F. Q. Chen, R. D. Chen, J. Q. Li, L. D. Guo, Y. Liu, F. X. Shen, Q. W. Yang, Z. G. Zhang, Q. L. Ren and Z. B. Bao, *Small*, 2023, **19**, 2208182.
- 35 Q. Dong, X. Zhang, S. Liu, R. B. Lin, Y. Guo, Y. Ma, A. Yonezu, R. Krishna, G. Liu, J. Duan, R. Matsuda, W. Jin and B. Chen, *Angew. Chem., Int. Ed.*, 2020, **59**, 22756–22762.
- 36 Q. Dong, Y. Huang, K. Hyeon-Deuk, I. Y. Chang, J. Wan, C. Chen, J. Duan, W. Jin and S. Kitagawa, *Adv. Funct. Mater.*, 2022, **32**, 2203745.
- 37 Y. Huang, J. Wan, T. Pan, K. Ge, Y. Guo, J. Duan, J. Bai, W. Jin and S. Kitagawa, *J. Am. Chem. Soc.*, 2023, **145**, 24425–24432.
- 38 J. Wan, H. L. Zhou, K. Hyeon-Deuk, I. Y. Chang, Y. Huang, R. Krishna and J. Duan, *Angew. Chem., Int. Ed.*, 2023, **62**, e202316792.
- 39 H. Wang, Y. Duan, Y. Wang, Y. Huang, K. Ge, S. Wang, B. Zheng, Z. Wang, J. Bai and J. Duan, *ACS Appl. Mater. Interfaces*, 2022, **14**, 13550–13559.
- 40 Y. F. Duan, Y. H. Huang, C. Q. Wang, Q. Wang, K. Ge, Z. Y. Lu, H. J. Wang, J. G. Duan, J. F. Bai and W. Q. Jin, *Chem. Sci.*, 2023, **14**, 4605–4611.
- 41 H.-M. Wen, C. Yu, M. Liu, C. Lin, B. Zhao, H. Wu, W. Zhou, B. Chen and J. Hu, *Angew. Chem., Int. Ed.*, 2023, **62**, e202309108.
- 42 Q. Dong, Y. Huang, J. Wan, Z. Lu, Z. Wang, C. Gu, J. Duan and J. Bai, *J. Am. Chem. Soc.*, 2023, **145**, 8043–8051.
- 43 R. Fantoni, K. Vanhelvoort, W. Knippers and J. Reuss, *Chem. Phys.*, 1986, **110**, 1–16.
- 44 Q. B. Dong, J. M. Wan, H. H. Chen, Y. H. Huang and J. G. Duan, *ACS Appl. Mater. Interfaces*, 2023, **15**, 39606–39613.

